JACS
JOURNAL OF THE AMERICAN CHEMICAL SOCIETY
Article
pubs.acs.org/JACS

# Turn Plasticity Distinguishes Different Modes of Amyloid-β Aggregation

Nasrollah Rezaei-Ghaleh,[†,‡] Mehriar Amininasab,[§] Karin Giller,[‡] Sathish Kumar,[⊥] Anne Stündl,[¶] Anja Schneider,[†,∥,¶,#] Stefan Becker,[‡] Jochen Walter,[⊥] and Markus Zweckstetter*[,†,‡,∥]

[†]German Center for Neurodegenerative Diseases (DZNE), 37077 Göttingen, Germany
[‡]Department for NMR-based Structural Biology, Max Planck Institute for Biophysical Chemistry, 37077 Göttingen, Germany
[§]Department of Cell and Molecular Biology, School of Biology, College of Science, University of Tehran, Tehran, Iran
[⊥]Department of Neurology, University of Bonn, 53127 Bonn, Germany
[∥]Center for Nanoscale Microscopy and Molecular Physiology of the Brain, University Medical Center, University of Göttingen, 37073 Göttingen, Germany
[¶]Department of Psychiatry and Psychotherapy, University Medicine Göttingen, 37075 Göttingen, Germany
[#]Max Planck Institute for Experimental Medicine, 37075 Göttingen, Germany

Supporting Information

**ABSTRACT:** Pathogenesis of Alzheimer's disease (AD) is associated with aggregation of the amyloid-β (Aβ) peptide into oligomeric and fibrillar assemblies; however, little is known about the molecular basis of aggregation of Aβ into distinct assembly states. Here we demonstrate that phosphorylation at serine 26 (S26) impairs Aβ fibrillization while stabilizing its monomers and nontoxic soluble assemblies of nonfibrillar morphology. NMR spectroscopy and replica-exchange molecular dynamics indicate that introduction of a phosphate group or phosphomimetic at position 26 diminishes Aβ's propensity to form a β-hairpin, rigidifies the region around the modification site, and interferes with formation of a fibril-specific salt bridge between aspartic acid 23 and lysine 28. The combined data demonstrate that phosphorylation of S26 prevents a distinct conformational rearrangement that is required for progression of Aβ aggregation toward fibrils and provide a basis for a possible role of phosphorylation at serine 26 in AD.

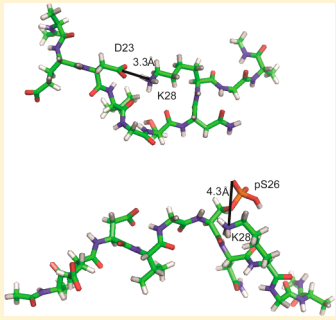


## INTRODUCTION

Deposition of the amyloid-β (Aβ) peptide as extracellular senile plaques in brain is a pathological hallmark of Alzheimer's disease (AD).[1] Conversion of soluble monomeric Aβ into insoluble amyloid fibrils involves formation of metastable intermediate structures of various sizes,[2] including Aβ dimers,[3] Aβ-derived diffusible ligands (ADDL),[4] globulomers,[5] Aβ*56,[6] and annular protofibrils.[7] A growing body of evidence supports the view that oligomers rather than mature amyloid fibrils are the main toxic species of AD,[8,9] in line with the finding that clinical AD presentation is only poorly correlated with amyloid plaque load.

Monomeric Aβ is intrinsically disordered in aqueous solution.[10,11] After conversion into fibrils, two β-strands are formed (Figure 1).[12−15] The intervening region comprising residues 25−29 forms a bend-like structure that juxtaposes the hydrophobic faces of the two cross-β units (Figure 1). Formation of a turn by residues 25−29 is important for pathogenic aggregation of Aβ as supported by several experimental and computational studies.[16−23] In addition, mutations just before the turn region, such as Italian (E22K), Arctic (E22G), Dutch (E22Q), Osaka (E22Δ), and Iowa (D23N) variants, alter the aggregation propensity of Aβ and cause early onset familial AD.[24] For some E22 variants, enhanced aggregation was attributed to the removal of a negative charge at position 22 and subsequent promotion of a salt bridge between D23 and K28—a distinct salt bridge in the structural core of Aβ fibrils (Figure 1).[17,19] β-Hairpin formation of residues L17-V36 early during Aβ aggregation was further supported by the structure of Aβ in complex with an affibody,[25] and a turn-like structure of residues 25−29 was found in Aβ oligomers.[26]

Besides inherited mutations within the Aβ sequence, cytotoxic Aβ aggregation is influenced by a variety of post-translational modifications. C-Terminal truncation strongly influences Aβ aggregation,[27] and an increase in Aβ42/Aβ40 ratio is associated with AD.[1] N-Truncation with or without pyroglutamate formation at E3 or E11 also promotes Aβ aggregation and has been connected to AD.[28,29] We showed that phosphorylation at S8 enhances Aβ aggregation and fibrillization in vitro and in vivo.[30] Aβ can also be phosphorylated at a second site, S26, by the cdc2 kinase, and pS26-Aβ was found in neuronal extracts and AD brain.[31,32] In

**Received:** July 22, 2013
**Published:** March 11, 2014

  

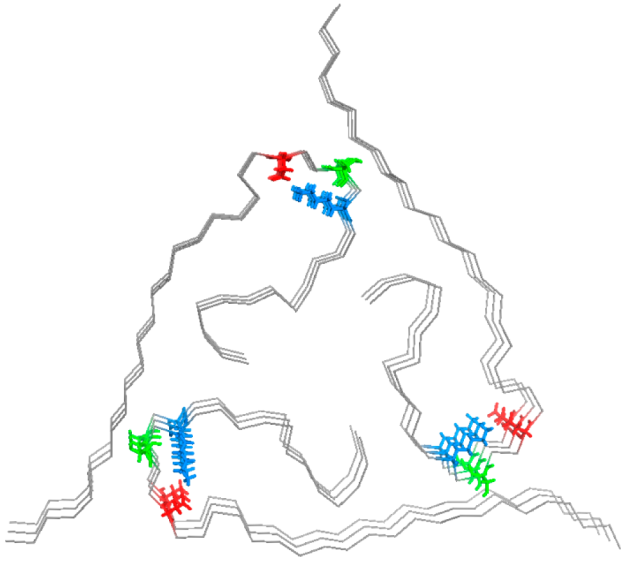

**Figure 1.** Structural model of brain-seeded A$\beta$ fibrils (PDB code: 2M4J[15]). Side chains of D23 (red) and K28 (blue), forming a salt bridge, and S26 (green) within the bend motif are marked.

addition, racemization of Ser and Asp residues of A$\beta$ occurs in senile plaques, and A$\beta$40 racemized at S26, in contrast with A$\beta$40 racemized at aspartates or S8, is incapable of forming fibrils and is susceptible to proteolysis yielding toxic fragments in vitro and in vivo.[33] The importance of residue 26 in A$\beta$ is further supported by its (and of G25) particular sensitivity to fibrillar destabilizing effect of proline replacements[34] and the finding that linkage between two A$\beta$ molecules at position 26 through oxidation of S26C mutants leads to formation of protofibril-like structures, rather than typical amyloid fibrils.[35]

Here we studied the importance of residue 26 for modulation of A$\beta$ aggregation. We show that A$\beta$40 phosphorylated at S26 does not form fibrils but retains its ability to form nonfibrillar assemblies. A combination of NMR spectroscopy and replica-exchange molecular dynamics demonstrates that the specific aggregation behavior of pS26-A$\beta$40 is due to impairment of a fibril-specific salt bridge between the side chains of D23 and K28. The combined data indicated that specific conformational rearrangements of residues 25−29 are essential for progression of A$\beta$ aggregation toward fibrils.

## EXPERIMENTAL SECTION

**Materials.** Synthetic wild-type (wt) A$\beta$40, pS26-A$\beta$40, and S26D-A$\beta$40 were obtained from Peptide Specialty Laboratory (Germany) and EZBiolab (USA). A$\beta$ peptides were solubilized in 10 mM NaOH at a concentration of 2 mg/mL (~460 $\mu$M), as recommended in ref 11, to minimize the amount of preformed aggregates and stored at −80 °C until use.

**Cloning, Expression, and Purification of Human A$\beta$40.** A DNA duplex coding for wt-, S26D-, and S26C-A$\beta$40 was cloned into a modified pET28a vector coding for an N-terminal TEV-protease-cleavable $His_6$-Z-tag fusion protein.[36] $^{15}N$,$^{13}C$-Labeled wt-, S26D-, and S26C-A$\beta$40 fusion proteins were expressed in *Escherichia coli* at 37 °C in Toronto minimal medium. After purification on a 1 mL HisTrap HP nickel column (GE Healthcare), the fusion protein was digested overnight on ice with recombinant TEV protease. The digestion mixture was loaded on a C4 reversed-phase Vydac HPLC column. The released A$\beta$40 peptide eluted from this column in a linear (0−100%) acetonitrile gradient as a single peak. According to electrospray mass spectrometry, the isolated peptide was 100% pure. The purified peptide was lyophilized before use. Lyophilized peptide was solubilized in 10 mM NaOH as described above.

**Thioflavin T (ThT) Fluorescence Measurements.** Samples of synthetic wt-A$\beta$40, pS26-A$\beta$40, and S26D-A$\beta$40 (~50 $\mu$M peptide concentration in 25 mM phosphate buffer, 50 mM NaCl, pH 7.4) were incubated at 37 °C with gentle stirring. Kinetics of A$\beta$ aggregation were followed by addition of 10 $\mu$L from the A$\beta$40 samples to 2 mL of 25 $\mu$M ThT solutions at the specified time points, followed by measurement of ThT emission intensity. Excitation and emission wavelengths were 446 and 485 nm, respectively, with slits of 10 nm each.

**Circular Dichroism (CD) Spectroscopy.** CD measurements were performed on a Chirascan spectropolarimeter (Applied Photophysics, UK) using a cuvette of 1 mm path length. After solubilization in 100 mM NaOH, synthetic A$\beta$40, pS26-A$\beta$40, and S26D-A$\beta$40 were dissolved in 25 mM sodium phosphate (pH 7.4, 50 mM NaCl) at a concentration of 0.15 mg/mL. Before and after 3 days of incubation at 37 °C with gentle stirring, CD spectra were recorded at 20 °C, from 260 to 190 at 0.5 nm intervals.

**Dynamic Light Scattering (DLS).** DLS experiments were performed on a DynaPro Titan (Wyatt Technology Corp., CA, USA) instrument, with a laser of 827.08 nm and a scattering angle of 90°. 100 $\mu$M peptide solutions (in 25 mM phosphate buffer, 50 mM NaCl, pH 7.4) were incubated for 2 days at 37 °C with stirring, and then centrifuged at 16 000$g$ for 30 min, and the supernatant was taken for DLS measurements. The size distribution was determined by constrained regularization.

**Monomer Consumption Assay.** One-dimensional $^{1}H$ NMR spectra of A$\beta$ peptides were measured at 37 °C before and after incubation at the specified time points in the aggregation condition (37 °C with gentle stirring). After chemical shift referencing by an external 4,4-dimethyl-4-silapentane-1-sulfonic acid (DSS) reference, the integrated intensity of $^{1}H$ peaks from 0.65 to 1.00 ppm and from 6.50 to 7.50 ppm was calculated. Subsequent to intensity normalization on the basis of the integrated intensity of the DSS peak, the relative intensity of the peptide $^{1}H$ peaks was used to monitor peptide monomer consumption during the early phases of A$\beta$ aggregation.

**Atomic Force Microscopy (AFM).** Fifty microliters of wt-A$\beta$40 and pS26-A$\beta$40 samples, which had been incubated for 2 days in the aggregation condition, was allowed to be adsorbed onto the surface of freshly cleaved mica coverslips. After 10 min, the surface was washed with water and dried three times. AFM imaging was performed in tapping mode using a MFP-3D AFM machine (Asylum Research, Santa Barbara, CA, USA).

**NMR Spectroscopy.** All NMR spectra were recorded at 278 K and pH 7.2, buffered with 20 mM sodium phosphate, on Bruker spectrometers (Germany) with $^{1}H$ Larmor frequencies of 600, 700, and 800 MHz. Chemical shift referencing at this temperature and pH was made with respect to the external DSS signal (0.0 ppm). Backbone resonance assignments were obtained through conventional homonuclear $^{1}H$,$^{1}H$ TOCSY and NOESY and heteronuclear $^{1}H$,$^{15}N$ HSQC, HNHA, HNCA, HNCO, and CBCA(CO)NH spectra (for a review, see ref 37). The mixing time in the NOESY experiment was 200 ms. To calculate secondary chemical shifts, random coil shifts were predicted according to ref 38. All NMR spectra were processed and analyzed using NMRPipe[39] and Sparky3.[40]

The $^{15}N$ longitudinal and transverse relaxation rates, $R_1$ and $R_2$, the longitudinal relaxation rate in the rotating frame ($R_{1\rho}$), and steady-state $^{1}H$,$^{15}N$ heteronuclear NOE[41] values were measured on a Bruker 600 MHz spectrometer with a room temperature probe. Relaxation delays of 8, 40, 80, 200, 400, 600, and 1000 ms for $R_1$ and 10, 30, 70, 110, 160, 240, and 320 ms for $R_2$ were used. $R_{1\rho}$ rates were measured using a $^{15}N$ spin-lock field strength of 2.5 kHz and relaxation delays of 10, 40, 70, 110, 160, 240, 320, 400, and 500 ms. The spin-lock frequency was set to the middle of the sweep width in the $^{15}N$ dimension. Heteronuclear NOEs between $^{1}H$ and $^{15}N$ were measured with a 3.5 s irradiation of protons. All relaxation measurements were performed in an interleaved manner. For $R_2$ and $R_{1\rho}$, a heat compensation element was implemented before the recycle delay.


dx.doi.org/10.1021/ja411707y | J. Am. Chem. Soc. 2014, 136, 4913−4919

The $^{15}$N exchange-mediated relaxation rate ($R_{ex}$) was estimated as the difference between $R_2$ and $R_{1\rho}$.

Water-amide proton exchange rates were measured using CLEANEX-PM-FHSQC experiments.[42] Selective water excitation was followed by a mixing time ($\tau_m$) of increasing duration (8, 16, 24, 32, 48, 75, 100, 200, and 500 ms) during which chemical exchange between water and NH protons took place. The normalized rate constant, $k$, related to the forward exchange rate constant between water and NH protons was calculated as described in ref 42.

Pulse field gradient-stimulated echo (PFG-STE) diffusion experiments were measured using 50 $\mu$M A$\beta$ samples in phosphate buffer (20 mM, pH 7.2) at 5 °C.[43] The sample contained dioxane as an internal hydrodynamic radius standard and viscosity probe.[44] A gradient distance (big delta) of 200 ms and total gradient length (little delta) of 4 ms were used. Gradient calibration was based on the measurement of the diffusion of residual HDO in 99.8% $D_2O$ at 298 K.

**Replica-Exchange Molecular Dynamic (REMD) Simulation.** Molecular dynamics simulations were performed using the Amber99sb force field[45] as implemented in GROMACS.[46] The starting structures of nonphosphorylated and S26-phosphorylated A$\beta_{21-30}$ were built in an extended conformation. The N- and C-terminal residues were capped by acetylation and carboxamidation, respectively. Each peptide was solvated with 4850 TIP4P-Ew water molecules. System charges were neutralized by adding monovalent ions. Successive application of energy minimization and short length (1 ns) position restrained isothermal–isobaric simulation at 278 K was utilized to remove atomic clashes and adjust densities.

To improve conformational space sampling and convergence at lower temperatures, we used the replica-exchange method. Sixty-four identical copies of initial models (i.e., replicas), exponentially spaced over an optimized range of temperatures (278–460 K), were simulated in parallel at a constant volume with exchange attempts every 1 ps. The acceptance ratio between replicas of adjacent temperatures ranged from 20 to 40%. The LINCS algorithm was used to constrain bonds.[47] A time step of 2 fs was chosen for integration. Coupling to a V-rescale heat bath maintained the specified temperatures. CA, CB, and CO shifts were calculated using SHIFTX2.[48] Cluster analysis was performed using a cutoff root mean square deviation (rmsd) of 0.1 nm. The most abundant clusters were visualized using PyMol (DeLano, W.L. The PyMOL Molecular Graphics System (2002) DeLano Scientific, San Carlos, CA, USA).

## RESULTS

**Phosphorylation at Serine 26 Targets A$\beta$ into Nonfibrillar Assemblies.** A$\beta$ can be phosphorylated at serine 26 in vivo.[31] To investigate its effect on misfolding of A$\beta$, we incubated wt-A$\beta$40 and pS26-A$\beta$40 peptide solutions under aggregation-promoting conditions. Following a lag phase of ~4 h, ThT emission intensity of wt-A$\beta$40 increased, in agreement with a nucleation-dependent mechanism (Figure 2a). In contrast, ThT emission intensity of pS26-A$\beta$40 remained nearly constant up until ~12 h and showed only a slight increase even after 30 h of incubation, in line with a previous observation.[32]

According to atomic force microscopy, wt-A$\beta$40 formed fibrils of up to 10–12 nm in diameter, while for pS26-A$\beta$40, only globular species of various sizes were observed (Figure 2b and Supporting Information Figure S1). Notably, we could not overcome the inability of pS26-A$\beta$40 to form $\beta$-sheet-rich fibrillar aggregates at higher peptide concentrations and longer incubation times (Figure S2), suggesting that the lack of pS26-A$\beta$40 fibrils is not caused by a kinetic barrier against aggregate formation.

Next, we monitored peptide monomer consumption using NMR spectroscopy. Conversion of A$\beta$ monomers to oligomers decreases the observable NMR signal due to line broadening. Indeed, for pS26-A$\beta$40, a 10% loss of signal intensity was

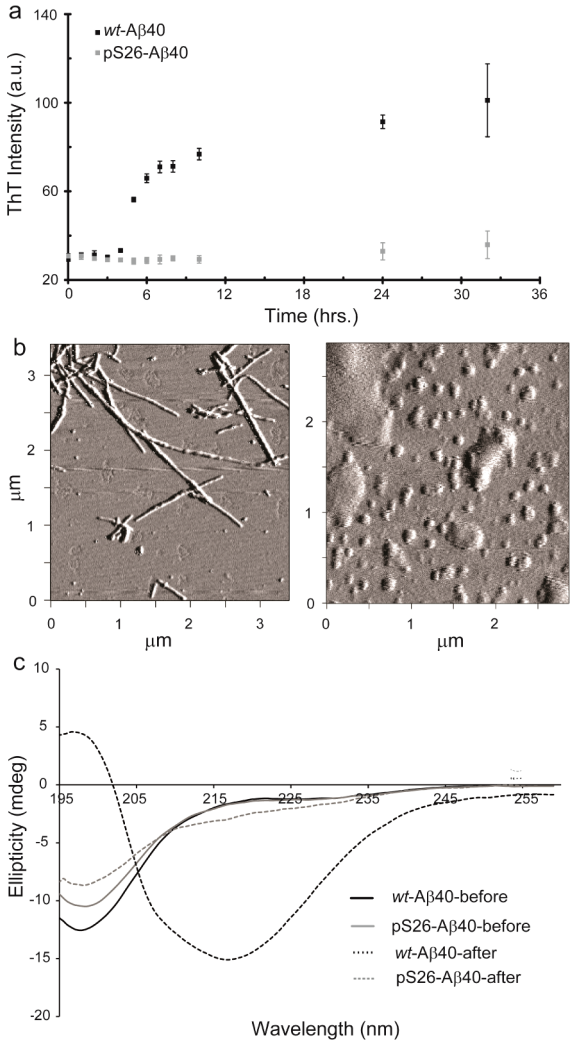


**Figure 2.** Phosphorylation at S26 prohibits A$\beta$40 aggregation into $\beta$-sheet-rich fibrils but allows A$\beta$40 assembly into nonfibrillar aggregates. (a) Evolution of ThT fluorescence emission intensity over the course of incubation of wt- and pS26-A$\beta$40 in an aggregation-promoting condition. (b) AFM images of A$\beta$40 after 2 days of aggregation; pS26-A$\beta$40 (right) is unable to form fibrillar aggregates, in contrast to wt-A$\beta$40 (left). (c) Far-UV CD spectra of A$\beta$40 variants during aggregation.

observed during a 24 h incubation period at 37 °C in the NMR tube (Figure S3a). Under more aggregation-prone conditions (as used in CD and ThT experiments; see below), the amount of aggregated pS26-A$\beta$40 increased to 20% (Figure S3b). In line with aggregation of pS26-A$\beta$40, light scattering intensity increased during the first 2 h of incubation (Figure S4a), and soluble nonfibrillar assemblies of pS26-A$\beta$40 with a hydrodynamic radius of approximately 100 nm were found after 24 h (Figure S4b). At the end of a 48 h period of aggregation, the supernatant of pS26-A$\beta$40 scattered light more strongly than either wt-A$\beta$40 or A$\beta$ phosphorylated at S8 (pS8-A$\beta$40) (Figure S4c), a variant with a high propensity to form oligomers and fibrils.[30] Far-UV circular dichroism furthermore showed that—after 3 days of aggregation and in contrast to wt-A$\beta$40—pS26-A$\beta$40 retained a CD spectrum that is characteristic for a largely disordered state (Figure 2c).

To investigate whether the nonfibrillar assemblies of pS26-A$\beta$40 are toxic, we performed MTT assays with primary cortical


dx.doi.org/10.1021/ja411707y | J. Am. Chem. Soc. 2014, 136, 4913–4919

neurons. While aggregated wt-A$\beta$40 resulted in decreased viability, no significant effect was observed after incubation of neurons with pS26-A$\beta$40 aggregates or monomers, indicating that the soluble nonfibrillar aggregates of pS26-A$\beta$40 were nontoxic (Figure S5).

**Conformational Dynamics at Serine 26.** To obtain insight into the aggregation properties of pS26-A$\beta$, we used a combination of NMR spectroscopy and molecular dynamics simulation. Due to the disordered nature of monomeric A$\beta$, NMR signal dispersion is low (Figure S6).[49,50] Estimation of the exchange contribution to the $^{15}$N transverse relaxation rate revealed a distinct dynamic behavior of residues S26 to G29. $R_{ex}$ values of S26, N27, and G29 exceeded those of neighboring residues (Figure S7 and Figure 3a), and the exchange rates of

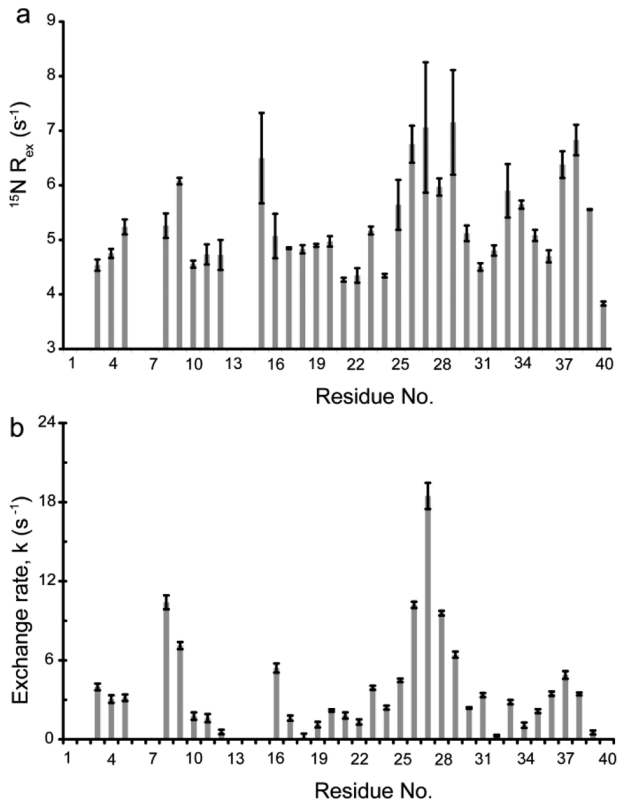


**Figure 3.** Conformational plasticity of residues G25−G29 in monomeric A$\beta$40. (a) Residue-specific exchange-mediated $^{15}$N transverse relaxation rates ($R_{ex}$) of monomeric A$\beta$40. Residues 25−29 show larger $R_{ex}$ than the rest of A$\beta$40, suggesting their involvement in conformational exchange dynamics. The higher $R_{ex}$ values of residues around H6, H13, and H14 are probably caused by changes in the protonation state of the histidine side chains. (b) Residue-specific water-amide proton exchange rates of A$\beta$40.

their amide protons were very large (Figure 3b), demonstrating that residues 26−29 experience strong conformational exchange in the disordered monomeric peptide.

NMR chemical shifts are highly sensitive probes for formation of secondary and tertiary polypeptide structure.[51] HA secondary chemical shifts of synthetic A$\beta$40 point to a slight but visible propensity for $\beta$-turn formation for residues E22−G25 (Figure 4a). Nuclear Overhauser enhancement (NOE) cross-peaks between D23 and G25, as well as between N27 and G29 (Figure 4b), further supported the presence of heterogeneous turn-like structures in the region that experiences strong conformational exchange (Figure 3).

Next, we asked how phosphorylation at S26 affects these conformational propensities. Figure S8 demonstrates that perturbations of NMR chemical shifts are restricted to the immediate vicinity of residue 26. Notably, the dispersion of the HB but not HD resonances of N27 was increased (Figure S9), suggesting that—although a detailed analysis of NOEs was hampered due to signal overlap—phosphorylation at S26 results in more rigid backbone conformations of N27. A decrease in dynamics was further supported by the intensity of the HN−HA correlation peak of N27, which rose by more than 2-fold in pS26-A$\beta$40; that is, the conformational exchange in the region 26−29 was strongly reduced upon phosphorylation at S26.

**Phosphorylation at Serine 26 Interferes with Formation of the D23−K28 Salt Bridge.** According to NMR, phosphorylation at S26 only influences the vicinity of the site of phosphorylation. We therefore performed replica-exchange molecular dynamic (REMD) simulations of the A$\beta$ fragment A21−A30 in its unphosphorylated and S26-phosphorylated forms at 278 K. Each replica was sampled for 20 ns. In line with sampling of mostly disordered conformations, carbon chemical shifts predicted from the simulation correlated with experimental values (Figure S10). Analysis of the conformations sampled during the simulation revealed that phosphorylation increased the end-to-end distances of A$\beta$(21−30) (Figure 4c), in line with the population of more extended states. In addition, phosphorylation decreased the propensity for turn/bend formation of residues E22−S26 (Figures 4d and S11). Inspection of the most populated clusters of each peptide provided a rationale for the observed changes. In the cluster of A$\beta$(21−30), a salt bridge between the side chains of D23 and K28 was present, the salt bridge that is a key feature of A$\beta$ fibrils,[12,13] and stabilizes a turn-like structure (Figure 4e). In contrast, the most abundant cluster of pS26-A$\beta$(21−30) does not contain this salt bridge. Instead, the positively charged side chain of K28 forms a salt bridge with the nearby phosphate group at residue 26. Due to the formation of this new salt bridge, the loop between residues 23−28 cannot be formed and the end-to-end distance of the peptide is increased.

**Phosphorylation Impairs Conformational Changes.** To provide additional support for the structural and dynamic changes induced by phosphorylation, we produced $^{15}$N,$^{13}$C-labeled protein of wt-A$\beta$40 and a phosphomimetic variant of A$\beta$40, in which S26 was mutated to aspartic acid. Phosphomimetic variants are particularly useful for in vivo studies, as they allow investigation of a defined phosphorylation state. The validity of S26D-A$\beta$40 is supported by REMD simulations: upon S26D mutation, the propensity of residues 22−26 to form bends/turns was diminished (Figure S11), and the salt bridge between the side chains of D23 and K28 was lost. Instead, the K28 side chain was located in proximity to the negatively charged side chain of D26 (Figure S11c). In addition, the S26D mutation prolonged the lag phase of A$\beta$ fibrillar aggregation (Figure S12).

Next we analyzed NMR chemical shifts in S26D-A$\beta$40. In line with the findings for pS26-A$\beta$40, chemical shift changes were restricted to residues around the site of mutation (Figure S13). According to the NMR analysis, residues D23−N27 have an increased propensity for extended conformations in S26D-A$\beta$40 (Figures 5a and S14).[52] In line with the specificity of the observed changes, an A$\beta$ variant in which S26 was mutated to cysteine (S26C-A$\beta$40) did not show—in reducing condition—a similar change (Figure S15). The NMR chemical shifts


dx.doi.org/10.1021/ja411707y | J. Am. Chem. Soc. 2014, 136, 4913−4919

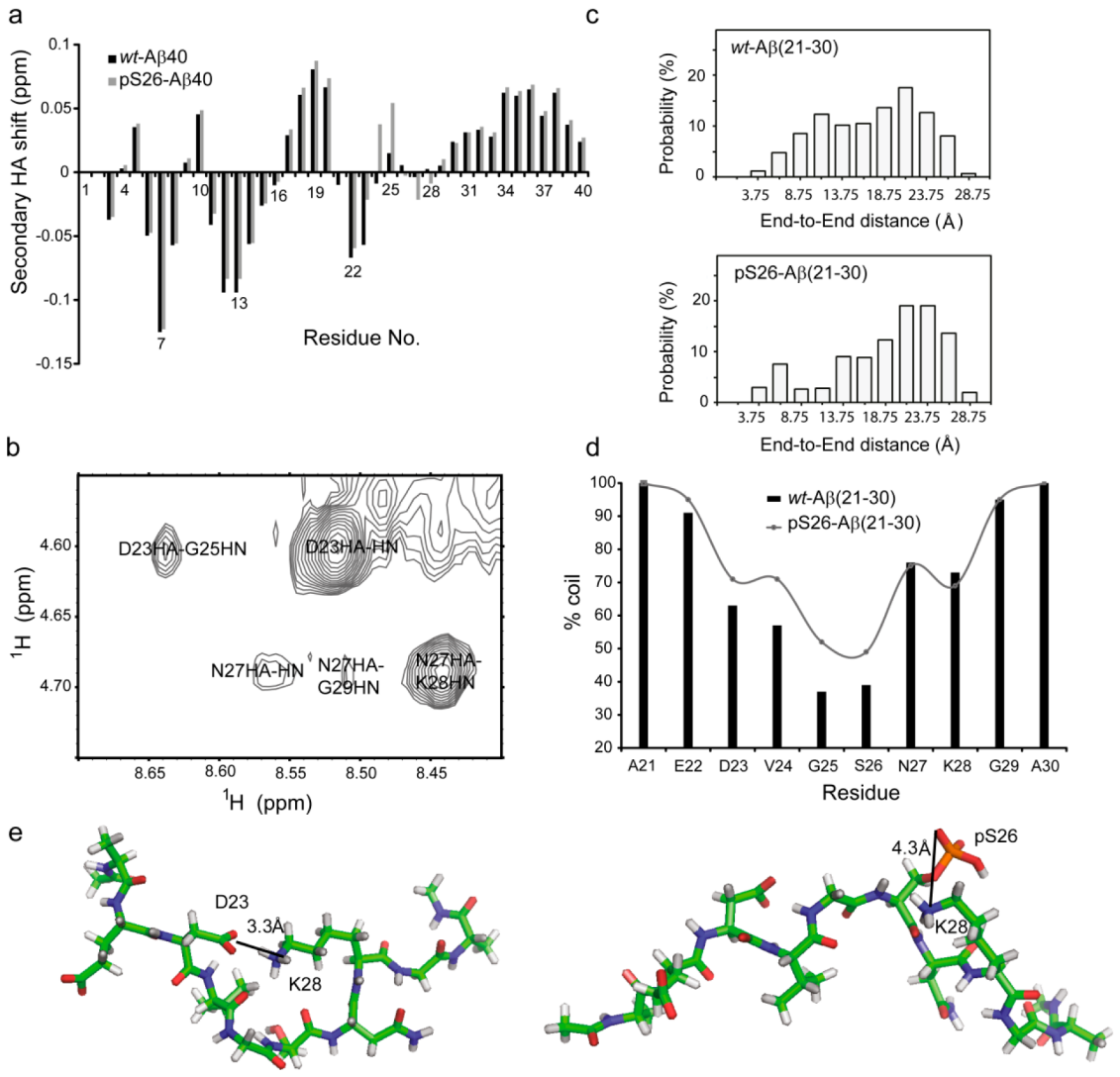


**Figure 4.** Phosphorylation of S26 impairs formation of the fibril-specific D23−K28 salt bridge. (a) HA secondary chemical shifts of wt- (black) and pS26-A$\beta$40 (gray). (b) Selected region of a 2D $^1$H,$^1$H NOESY spectrum of wt-A$\beta$40. Cross-peaks between the HN resonance of G25 and HA of D23, and between HA of N27 and HN of G29 point to a propensity of residues 22−25 and 26−29 for $\beta$-turn formation. (c) Histogram of end-to-end distances (distance between CA atoms of A21 and A30) obtained from MD simulations of A$\beta$(21−30) in the S26-phosphorylated and nonphosphorylated states. (d) Percentage of coil conformation observed in the MD ensemble of wt- and pS26-A$\beta$(21−30). (e) Representative structures of the highest-population cluster in the MD ensembles of wt- (left) and pS26-A$\beta$(21−30) (right).

further supported on the basis of the random coil index (RCI) order parameter that the mobility of residues D23−N27 was diminished in the S26D variant (Figure S16a).[53] In addition, changes in exchange-mediated contributions to NMR relaxation rates were consistent with rigidification of the A$\beta$ backbone: $^{15}$N $R_{ex}$ and water-amide proton exchange rates of S26-G29, which had the highest values in wt-A$\beta$40 (Figure 3), were strongly decreased in S26D-A$\beta$40 (Figures 5b and S16b). On the other hand, the S26C mutation did affect the backbone dynamics of A$\beta$ much less (Figure S17). The data demonstrate that the S26D phosphomimetic mutation decreases the backbone mobility of residues 25−29 on multiple time scales.

## DISCUSSION

Our study demonstrates that conformational rearrangements around serine 26 are required for conversion of A$\beta$ monomers to fibrils. Phosphorylation at S26, in the region that is most prone to conformational changes in monomeric A$\beta$, interferes with A$\beta$ aggregation into $\beta$-sheet-rich fibrils but allows formation of nonfibrillar assemblies. NMR spectroscopy and molecular dynamics simulations demonstrated that impaired fibrillization is associated with a reduced plasticity of the residue stretch G25−G29. Formation of a salt bridge between K28 and the phosphorylated residue S26 rigidifies the structure and interferes with formation of the salt bridge between the side chains of K28 and D23 and therefore $\beta$-hairpin formation. The D23−K28 salt bridge may thus be essential for fibrillization but not for oligomerization.

Formation and stabilization of the $\beta$-hairpin plays an important role in aggregation of A$\beta$.[12−14,25] In agreement with previous reports,[11,50] our NMR data indicate that monomeric A$\beta$ transiently adopts a $\beta$-hairpin conformation in solution (Figures 3, 4, 5, and S14). Stabilization of the $\beta$-hairpin conformation in the aggregated state shifts the equilibrium between $\beta$-hairpin and other monomer conformations toward the $\beta$-hairpin conformation. Indeed, when D23 and K28 are chemically constrained by a lactam bridge, the aggregation rate of A$\beta$ increases by 3 orders of magnitude.[54] The strong increase


dx.doi.org/10.1021/ja411707y | J. Am. Chem. Soc. 2014, 136, 4913−4919

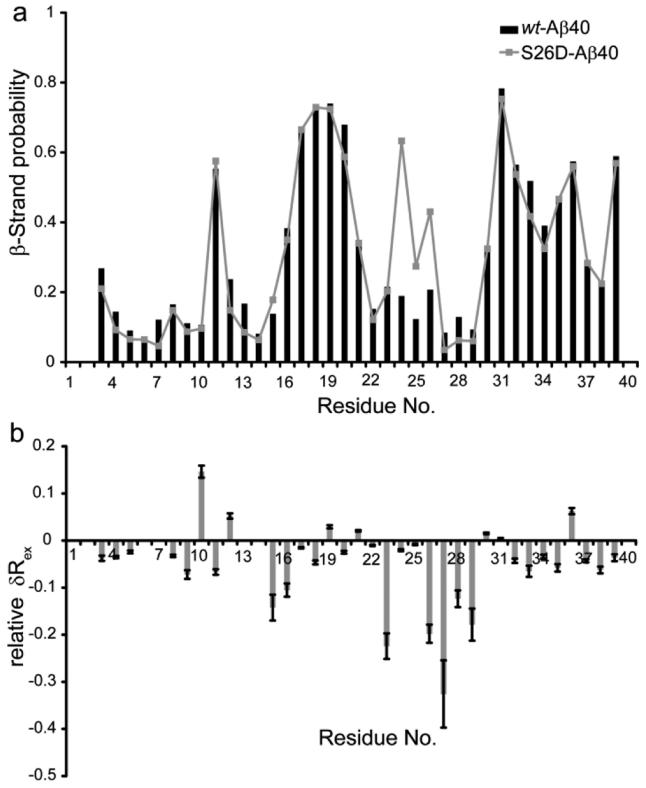


**Figure 5.** S26D phosphomimetic mutation decreases turn plasticity of A$\beta$40. (a) Probability score for $\beta$-strand conformation according to CA, CB, CO, N, HN, and HA chemical shifts[52] for wt- (black) and S26D-A$\beta$40 (gray). (b) Changes in exchange-mediated transverse relaxation rates ($R_{ex}$) upon S26D mutation. Residues 23−29 decrease in $R_{ex}$ after mutation, indicating that motions on the micro-to-millisecond time scale are diminished in this region.

in the aggregation rate is attributed to a decrease in entropic penalty of bend formation.[55] Moreover, the conformation formed by residues 25−29 can constitute a template over which a second A$\beta$ molecule adopts the same structure, stabilizing the $\beta$-hairpin and favoring A$\beta$ oligomerization.[23,25]

S26 is located at the center of the turn motif formed by residues G25−G29 (Figure 1). Introduction of a negatively charged phosphate group at this position will cause intermolecular repulsive interactions that lead to destabilization of the fibrillar conformation. Moreover, in some amyloid fibrils (including the recently reported brain-seeded A$\beta$40 fibrils[15]), the charged side chains of D23 and K28 would point to a low dielectric environment, which is thermodynamically unfavorable unless their charges are neutralized via a salt bridge. The impairment of the D23−K28 salt bridge by phosphorylation at S26 is therefore expected to result in thermodynamic instability of those A$\beta$ fibrils. Indeed, we found that even at very high peptide concentrations and long incubation periods amyloid fibrils were not formed (Figure S2). In contrast to amyloid fibrils, A$\beta$ preglobulomers and globulomers can contain a mixture of intramolecular antiparallel and intermolecular parallel $\beta$-sheets with G25−G29 constituting the connecting bend.[26] In the currently available structural models of A$\beta$ oligomers, S26 is not located in a tightly packed region. Thus, phosphorylation at S26 is expected to have a smaller, if any, destabilizing impact on A$\beta$ oligomers when compared to fibrils, in line with the observed nonfibrillar assembly of pS26-A$\beta$40 (Figures 2, S1, and S4).

A certain amount of plasticity in the G25−G29 turn region is required for conversion of oligomers into ordered fibrils.[2,56,57] In line with this hypothesis, enhanced aggregation of variants of A$\beta$ causing early onset AD, such as E22K, E22G, E22Q, and D23N, was linked to destabilization of the turn-like structure.[19] Moreover, overstabilization of the turn through chemical cross-linking of A21 and A30 in a double-cysteine mutant reduced fibril formation and stabilized neurotoxic A$\beta$ oligomers.[58] Our NMR data demonstrate that upon phosphorylation at S26 (Figure S9), as well as mutation to the phosphomimetic variant S26D (Figures 5, S16, and S17), residues 23−28 become more rigid. Due to the decreased turn plasticity of pS26-A$\beta$, fibrillization is impaired, whereas nonfibrillar aggregation can still occur. Consistent with this finding, constrained motion of residue 26 through introduction of an intermolecular disulfide bond blocked conversion of intermediate protofibril-like A$\beta$40 aggregates into typical amyloid fibrils.[35]

Post-translational modifications of A$\beta$ that enhance its cytotoxic aggregation are expected to contribute to the pathogenesis of late onset AD. Our data suggest that phosphorylation at S26 suppresses the formation of toxic oligomers and fibrils while stabilizing monomers and nontoxic soluble assemblies of nonfibrillar morphology. We have recently shown that phosphorylation of A$\beta$ at S8 by extracellular protein kinases promotes cytotoxic aggregation of A$\beta$.[30] In contrast to pS26-A$\beta$, A$\beta$ phosphorylated at S8 showed a high propensity to form $\beta$-sheet-rich oligomers and fibrils,[30] indicating that phosphorylation of A$\beta$ at distinct sites can lead to drastically different consequences on pathogenic aggregation. In addition, as phosphorylation at both S8 and S26 modulates A$\beta$ aggregation, targeting phosphorylation/dephosphorylation of A$\beta$ might offer new ways for prevention of late onset sporadic AD.

## CONCLUSION

We demonstrated that phosphorylation of A$\beta$ at S26 blocks conversion of A$\beta$ monomers to $\beta$-sheet-rich fibrils. Our findings highlight the importance of the plasticity of residues G25−G29 in the control of A$\beta$ aggregation and the role of the D23−K28 salt bridge in A$\beta$ fibrillization. Targeting the plasticity of residues G25−G29 by influencing phosphorylation of serine 26 might provide a therapeutic route for late onset sporadic AD.

## ASSOCIATED CONTENT

### Supporting Information

Supporting data as Figures S1−S17. This material is available free of charge via the Internet at http://pubs.acs.org.

## AUTHOR INFORMATION

### Corresponding Author

markus.zweckstetter@dzne.de

### Notes

The authors declare no competing financial interest.

## ACKNOWLEDGMENTS

We thank Alice Soragni for acquisition of 2D homonuclear spectra. This work was supported by DFG (ZW 71/2-2 and 3-2) to M.Z. and DFG (Grant WA1477/6-2) to J.W.

## REFERENCES

(1) Hardy, J.; Selkoe, D. J. *Science* **2002**, *297*, 353.
(2) Fandrich, M. *J. Mol. Biol.* **2012**, *421*, 427.

(3) Shankar, G. M.; Li, S.; Mehta, T. H.; Garcia-Munoz, A.; Shepardson, N. E.; Smith, I.; Brett, F. M.; Farrell, M. A.; Rowan, M. J.; Lemere, C. A.; Regan, C. M.; Walsh, D. M.; Sabatini, B. L.; Selkoe, D. J. *Nat. Med.* **2008**, *14*, 837.
(4) De Felice, F. G.; Velasco, P. T.; Lambert, M. P.; Viola, K.; Fernandez, S. J.; Ferreira, S. T.; Klein, W. L. *J. Biol. Chem.* **2007**, *282*, 11590.
(5) Gellermann, G. P.; Byrnes, H.; Striebinger, A.; Ullrich, K.; Mueller, R.; Hillen, H.; Barghorn, S. *Neurobiol. Dis.* **2008**, *30*, 212.
(6) Lesne, S.; Koh, M. T.; Kotilinek, L.; Kayed, R.; Glabe, C. G.; Yang, A.; Gallagher, M.; Ashe, K. H. *Nature* **2006**, *440*, 352.
(7) Lashuel, H. A.; Hartley, D.; Petre, B. M.; Walz, T.; Lansbury, P. T., Jr. *Nature* **2002**, *418*, 291.
(8) Stefani, M. *Prog. Neurobiol.* **2012**, *99*, 226.
(9) Glabe, C. G. *J. Biol. Chem.* **2008**, *283*, 29639.
(10) Riek, R.; Guntert, P.; Dobeli, H.; Wipf, B.; Wuthrich, K. *Eur. J. Biochem.* **2001**, *268*, 5930.
(11) Hou, L.; Shao, H.; Zhang, Y.; Li, H.; Menon, N. K.; Neuhaus, E. B.; Brewer, J. M.; Byeon, I. J.; Ray, D. G.; Vitek, M. P.; Iwashita, T.; Makula, R. A.; Przybyla, A. B.; Zagorski, M. G. *J. Am. Chem. Soc.* **2004**, *126*, 1992.
(12) Petkova, A. T.; Ishii, Y.; Balbach, J. J.; Antzutkin, O. N.; Leapman, R. D.; Delaglio, F.; Tycko, R. *Proc. Natl. Acad. Sci. U.S.A.* **2002**, *99*, 16742.
(13) Petkova, A. T.; Yau, W. M.; Tycko, R. *Biochemistry* **2006**, *45*, 498.
(14) Luhrs, T.; Ritter, C.; Adrian, M.; Riek-Loher, D.; Bohrmann, B.; Dobeli, H.; Schubert, D.; Riek, R. *Proc. Natl. Acad. Sci. U.S.A.* **2005**, *102*, 17342.
(15) Lu, J. X.; Qiang, W.; Yau, W. M.; Schwieters, C. D.; Meredith, S. C.; Tycko, R. *Cell* **2013**, *154*, 1257.
(16) Lazo, N. D.; Grant, M. A.; Condron, M. C.; Rigby, A. C.; Teplow, D. B. *Protein Sci.* **2005**, *14*, 1581.
(17) Borreguero, J. M.; Urbanc, B.; Lazo, N. D.; Buldyrev, S. V.; Teplow, D. B.; Stanley, H. E. *Proc. Natl. Acad. Sci. U.S.A.* **2005**, *102*, 6015.
(18) Baumketner, A.; Bernstein, S. L.; Wyttenbach, T.; Lazo, N. D.; Teplow, D. B.; Bowers, M. T.; Shea, J. E. *Protein Sci.* **2006**, *15*, 1239.
(19) Grant, M. A.; Lazo, N. D.; Lomakin, A.; Condron, M. M.; Arai, H.; Yamin, G.; Rigby, A. C.; Teplow, D. B. *Proc. Natl. Acad. Sci. U.S.A.* **2007**, *104*, 16522.
(20) Krone, M. G.; Baumketner, A.; Bernstein, S. L.; Wyttenbach, T.; Lazo, N. D.; Teplow, D. B.; Bowers, M. T.; Shea, J. E. *J. Mol. Biol.* **2008**, *381*, 221.
(21) Fawzi, N. L.; Phillips, A. H.; Ruscio, J. Z.; Doucleff, M.; Wemmer, D. E.; Head-Gordon, T. *J. Am. Chem. Soc.* **2008**, *130*, 6145.
(22) Murray, M. M.; Krone, M. G.; Bernstein, S. L.; Baumketner, A.; Condron, M. M.; Lazo, N. D.; Teplow, D. B.; Wyttenbach, T.; Shea, J. E.; Bowers, M. T. *J. Phys. Chem. B* **2009**, *113*, 6041.
(23) Larini, L.; Shea, J. E. *Biophys. J.* **2012**, *103*, 576.
(24) Tanzi, R. E. *Cold Spring Harbor Perspect. Med.* **2012**, 2.
(25) Hoyer, W.; Gronwall, C.; Jonsson, A.; Stahl, S.; Hard, T. *Proc. Natl. Acad. Sci. U.S.A.* **2008**, *105*, 5099.
(26) Yu, L.; Edalji, R.; Harlan, J. E.; Holzman, T. F.; Lopez, A. P.; Labkovsky, B.; Hillen, H.; Barghorn, S.; Ebert, U.; Richardson, P. L.; Miesbauer, L.; Solomon, L.; Bartley, D.; Walter, K.; Johnson, R. W.; Hajduk, P. J.; Olejniczak, E. T. *Biochemistry* **2009**, *48*, 1870.
(27) Jarrett, J. T.; Berger, E. P.; Lansbury, P. T., Jr. *Biochemistry* **1993**, *32*, 4693.
(28) Sullivan, C. P.; Berg, E. A.; Elliott-Bryant, R.; Fishman, J. B.; McKee, A. C.; Morin, P. J.; Shia, M. A.; Fine, R. E. *Neurosci. Lett.* **2011**, *505*, 109.
(29) Bouter, Y.; Dietrich, K.; Wittnam, J. L.; Rezaei-Ghaleh, N.; Pillot, T.; Papot-Couturier, S.; Lefebvre, T.; Sprenger, F.; Wirths, O.; Zweckstetter, M.; Bayer, T. A. *Acta Neuropathol.* **2013**, *126*, 189.
(30) Kumar, S.; Rezaei-Ghaleh, N.; Terwel, D.; Thal, D. R.; Richard, M.; Hoch, M.; McDonald, J. M.; Wullner, U.; Glebov, K.; Heneka, M. T.; Walsh, D. M.; Zweckstetter, M.; Walter, J. *EMBO J.* **2011**, *30*, 2255.
(31) Milton, N. G. *Subcell. Biochem.* **2005**, *38*, 381.
(32) Milton, N. G. *Neuroreport* **2001**, *12*, 3839.
(33) Kaneko, I.; Morimoto, K.; Kubo, T. *Neuroscience* **2001**, *104*, 1003.
(34) Williams, A. D.; Shivaprasad, S.; Wetzel, R. *J. Mol. Biol.* **2006**, *357*, 1283.
(35) O'Nuallain, B.; Freir, D. B.; Nicoll, A. J.; Risse, E.; Ferguson, N.; Herron, C. E.; Collinge, J.; Walsh, D. M. *J. Neurosci.* **2010**, *30*, 14411.
(36) Edlich, C.; Stier, G.; Simon, B.; Sattler, M.; Muhle-Goll, C. *Structure* **2005**, *13*, 277.
(37) Whitehead, B.; Craven, C. J.; Waltho, J. P. *Methods Mol. Biol.* **1997**, *60*, 29.
(38) Tamiola, K.; Acar, B.; Mulder, F. A. *J. Am. Chem. Soc.* **2010**, *132*, 18000.
(39) Delaglio, F.; Grzesiek, S.; Vuister, G. W.; Zhu, G.; Pfeifer, J.; Bax, A. *J. Biomol. NMR* **1995**, *6*, 277.
(40) Goddard, T. D.; Kneller, D. G. *SPARKY* 3; University of California, San Francisco.
(41) Palmer, A. G., III. *Annu. Rev. Biophys. Biomol. Struct.* **2001**, *30*, 129.
(42) Hwang, T. L.; van Zijl, P. C.; Mori, S. *J. Biomol. NMR* **1998**, *11*, 221.
(43) Johnson, C. S., Jr. *Prog. Nucl. Magn. Reson. Spectrosc.* **1999**, *34*, 203.
(44) Wilkins, D. K.; Grimshaw, S. B.; Receveur, V.; Dobson, C. M.; Jones, J. A.; Smith, L. J. *Biochemistry* **1999**, *38*, 16424.
(45) Hornak, V.; Abel, R.; Okur, A.; Strockbine, B.; Roitberg, A.; Simmerling, C. *Proteins* **2006**, *65*, 712.
(46) Berendsen, H. J. C.; Van Der Spoel, D.; Van Drunen, R. *J. Comput. Phys. Commun.* **1995**, *91*, 43.
(47) Hess, B.; Bekker, H.; Berendsen, H. J. C.; Fraaije, J. G. E. M. *J. Comput. Chem.* **1997**, *18*, 1463.
(48) Han, B.; Liu, Y.; Ginzinger, S. W.; Wishart, D. S. *J. Biomol. NMR* **2011**, *50*, 43.
(49) Yan, Y.; Wang, C. *J. Mol. Biol.* **2006**, *364*, 853.
(50) Rezaei-Ghaleh, N.; Giller, K.; Becker, S.; Zweckstetter, M. *Biophys. J.* **2011**, *101*, 1202.
(51) Wishart, D. S. *Prog. Nucl. Magn. Reson. Spectrosc.* **2011**, *58*, 62.
(52) Shen, Y.; Bax, A. *J. Biomol. NMR* **2012**, *52*, 211.
(53) Berjanskii, M. V.; Wishart, D. S. *J. Am. Chem. Soc.* **2005**, *127*, 14970.
(54) Sciarretta, K. L.; Gordon, D. J.; Petkova, A. T.; Tycko, R.; Meredith, S. C. *Biochemistry* **2005**, *44*, 6003.
(55) Reddy, G.; Straub, J. E.; Thirumalai, D. *J. Phys. Chem. B* **2009**, *113*, 1162.
(56) Habicht, G.; Haupt, C.; Friedrich, R. P.; Hortschansky, P.; Sachse, C.; Meinhardt, J.; Wieligmann, K.; Gellermann, G. P.; Brodhun, M.; Gotz, J.; Halbhuber, K. J.; Rocken, C.; Horn, U.; Fandrich, M. *Proc. Natl. Acad. Sci. U.S.A.* **2007**, *104*, 19232.
(57) Pellarin, R.; Guarnera, E.; Caflisch, A. *J. Mol. Biol.* **2007**, *374*, 917.
(58) Sandberg, A.; Luheshi, L. M.; Sollvander, S.; Pereira de Barros, T.; Macao, B.; Knowles, T. P.; Biverstal, H.; Lendel, C.; Ekholm-Petterson, F.; Dubnovitsky, A.; Lannfelt, L.; Dobson, C. M.; Hard, T. *Proc. Natl. Acad. Sci. U.S.A.* **2010**, *107*, 15595.